

Coulomb interactions in systems of generalized semi-Dirac fermions

Mohamed M. Elsayed,¹ Bruno Uchoa,² and Valeri N. Kotov¹

¹*Department of Physics, University of Vermont, Burlington, VT 05405, USA*

²*Department of Physics and Astronomy, Center for Quantum Research and Technology, University of Oklahoma, Norman, OK 73019, USA*

(Dated: November 12, 2024)

Interactions have strong effects in systems with flat bands. We examine the role of Coulomb interactions in two dimensional chiral anisotropic quasiparticles that disperse linearly in one direction and have relatively flat bands near the neutrality point in the other direction, dispersing with an arbitrary positive even power law $2n \geq 2$. As in the conventional semi-Dirac case ($n = 1$), we show using renormalization group that strong logarithmic divergences in the self-energy of generalized semi-Dirac fermions resum and lead to a restoration of the linearity of the spectrum for arbitrary n over a sizable energy window in the perturbative regime. We discuss those results in light of previous non-perturbative large N_f results and address the implications for physical observables.

I. INTRODUCTION

Semi-Dirac fermions are highly anisotropic quasiparticles in two dimensions that disperse as relativistic fermions in one direction and as massive Galilean invariant particles in the perpendicular direction. Type-I semi-Dirac fermions arise from a topological Lifshitz transition where two Dirac cones merge, resulting in a 2π Berry phase around the touching points of the conduction and valence bands. In the quantum Hall regime, semi-Dirac fermions have a signature $B^{2/3}$ scaling of the energy of the Landau levels with the applied magnetic field [1, 2], reflecting a sublinear zero-field scaling of the density of states (DOS) with energy around the touching point. Semi-Dirac fermions have been experimentally observed in black phosphorus under doping [3, 4], in nodal-line semimetal ZrSiS [5] and predicted to exist in strained honeycomb lattices [6], BEDT-TTF₂I₃ salt under pressure [7], and VO₂/TO₂ heterostructures [8, 9].

Short range interactions were theoretically found to drive the system to possible modulated ordered phases in the charge, spin and superconducting sectors, in the vicinity of a quantum critical point [10–13]. On the other hand, long range Coulomb interactions are known to strongly renormalize the spectrum of semi-Dirac fermions. Unlike in the case of conventional Dirac fermions in 2D [14], where self-energy corrections have a single leading logarithmic divergence in the infrared, the self-energy corrections for semi-Dirac fermions have an unconventional leading log squared infrared divergence [15–17]. Previous non-perturbative calculations in the large N_f limit, with N_f the fermionic degeneracy, have found a strong coupling non-Fermi liquid regime over a wide energy range followed by a perturbative marginal Fermi liquid in the vicinity of the fixed point [15]. A perturbative renormalization group calculation by some of us [17] identified an unusual regime where resummation of the log square divergences leads to restoration of the linearity of the spectrum over a wide energy window, making semi-Dirac fermions effectively behave as conventional anisotropic Dirac particles away from the

neutrality point.

Interaction effects have been recently shown to have prominent features and many-body instabilities in systems with flat bands [18–22]. In this paper, we consider the role of Coulomb interactions in 2D anisotropic systems with quasiparticles that disperse relativistically in one direction and have relatively flat bands with arbitrary curvature along the normal direction. We address the nature of the different perturbative regimes in systems of generalized semi-Dirac fermions, where the Hamiltonian has the form

$$\hat{\mathcal{H}}(\mathbf{p}) = h_x(\mathbf{p})\sigma_x + h_y(\mathbf{p})\sigma_y \equiv \frac{g_n}{2}p_x^{2n}\sigma_x + vp_y\sigma_y, \quad (1)$$

where σ_i ($i = x, y$) are the standard off-diagonal Pauli matrices, and $n \in \mathbb{N}$ controls the flatness of the dispersion along the p_x direction. v is the velocity of the quasiparticles dispersing along the p_y direction, which are massless, and g_n determines the curvature of the bands along the orthogonal direction. $n = 1$ corresponds to the standard dispersion for conventional semi-Dirac fermions. Similar generalizations have been proposed in the literature, whereby in Ref. [13] they study the effects of short range interactions in the one dimensional limit $n \rightarrow \infty$; in Ref. [23] they consider the topological charge

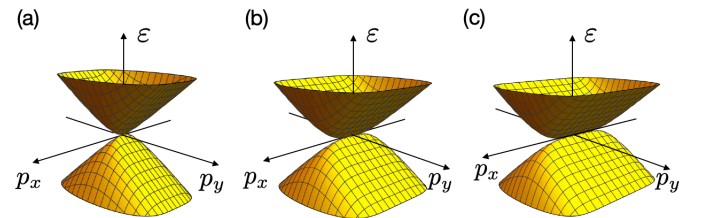


FIG. 1. a) Spectrum of semi-Dirac fermions ($n = 1$), which disperse linearly in one direction and parabolically in another. Generalized semi-Dirac fermions with b) $n = 2$ and c) $n = 3$. The energy spectrum becomes increasingly flat along the p_x direction around the touching point of the bands for larger n values. The DOS scales with energy as $\rho(\epsilon) \propto \epsilon^{\frac{1}{2n}}$. (see text).

of the band crossing for different members of this class of Hamiltonians; and in Ref. [24] they compute optical and DC conductivities. In the present work, we focus on renormalization of the spectrum due to both the long range and screened Coulomb interaction, and investigate the different perturbative regimes therein. This construction provides an analytical tool to compare the effects of electron-electron interactions in increasingly anisotropic Hamiltonians where the dispersion flattens out in one direction, remaining linear in the other. Moreover, it allows us to observe how screening is affected by the curvature of the bands.

The density of states for the free fermions scales as $\rho(\varepsilon) \propto \varepsilon^{\frac{1}{2n}}$ and is significantly enhanced near $\varepsilon \rightarrow 0$ for $n > 1$ as the dispersion along the p_x direction flattens out. In a strong transverse magnetic field, the Landau level spectrum scales as $\varepsilon \propto B^{2n/(2n+1)}$. A more detailed calculation of the physical observables is given in Section V.

We show that under the bare Coulomb interaction, restoration of linearity in the spectrum previously found for semi-Dirac fermions [17] persists for arbitrary $n > 1$ over an energy window

$$\varepsilon_n < \varepsilon < \Lambda e^{-\sqrt{\frac{n}{2n-1}}\pi/\alpha}, \quad (2)$$

where Λ is the ultraviolet energy cut-off, and $\alpha = e^2/v < \pi$ is a dimensionless coupling constant in the perturbative regime. The infrared cut-off $\varepsilon_n \sim vq_n(\alpha N_f)^{2n/(2n-1)}$ signals the onset of a regime where screening effects become dominant, where $q_n = (2v/g_n)^{1/(2n-1)}$ is the characteristic momentum. In the ultra-low energy regime $\varepsilon \ll \varepsilon_n$ our results are in agreement with the marginal-Fermi liquid behavior found in Ref. [15] for $n = 1$ in the vicinity of the weak coupling fixed point.

The paper is organized in the following way: in Section II we describe the perturbative one-loop self energy for generalized semi-Dirac fermions. In Section III we address the perturbative renormalization group (RG) analysis for arbitrary n , where leading log square divergences resum, leading to restoration of the linearity in the spectrum. In Section IV, we examine the ultra-low energy regime of generalized semi-Dirac fermions and in Section V we calculate the renormalization of physical observables in the zero field limit. Finally in Section VI we present a discussion of the different perturbative regimes in comparison with previous findings in the large N_f limit and present our conclusions.

II. PERTURBATIVE ONE-LOOP SELF-ENERGY

We start by calculating the one loop self-energy

$$\hat{\Sigma}(\mathbf{p}) = \frac{i}{(2\pi)^3} \int_{-\infty}^{\infty} d\omega \int d^2\mathbf{k} \hat{G}_0(\mathbf{k}, \omega) V(\mathbf{k} - \mathbf{p}), \quad (3)$$

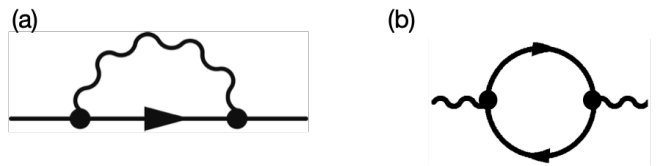


FIG. 2. a) Leading self-energy correction in perturbation theory. b) One loop polarization bubble. Wavy lines are undressed Coulomb interactions. Solid straight lines are fermionic propagators.

shown in Fig. 2a), where

$$\hat{G}_0(\mathbf{k}, \omega) = \left[\omega - \hat{\mathcal{H}}(\mathbf{k}) + i0^+ \text{sgn}(\omega) \right]^{-1} \quad (4)$$

is the time-ordered Green's function defined in terms of the Hamiltonian (1) and

$$V(\mathbf{k}) = \frac{2\pi e^2}{|\mathbf{k}|} \quad (5)$$

is the electron-electron Coulomb interaction. The frequency integral is easily performed to yield:

$$\hat{\Sigma}(\mathbf{p}) = \Sigma_x(\mathbf{p})\sigma_x + \Sigma_y(\mathbf{p})\sigma_y, \quad (6)$$

where

$$\Sigma_i(\mathbf{p}) = \frac{\pi}{(2\pi)^3} \int d^2\mathbf{k} \frac{h_i(\mathbf{k})}{\sqrt{h_x^2(\mathbf{k}) + h_y^2(\mathbf{k})}} V(\mathbf{k} - \mathbf{p}), \quad (7)$$

with $i = x, y$.

A. Velocity self-energy correction

We expand the potential for small external \mathbf{p} ($p \ll k$), retaining terms up to first order (the leading behavior in p_y)

$$V(\mathbf{k} - \mathbf{p}) \approx \frac{2\pi e^2}{k} \left(1 + \frac{\mathbf{k} \cdot \mathbf{p}}{k^2} \right). \quad (8)$$

By parity, only the term proportional to $k_y p_y$ contributes to the integral that gives $\Sigma_y(\mathbf{p})$ in Eq.(7). We transform to new coordinates defined by

$$\frac{g_n}{2} k_x^{2n} = \varepsilon \sin \phi, \quad vk_y = \varepsilon \cos \phi, \quad (9)$$

such that

$$\varepsilon = \sqrt{\left(\frac{g_n}{2} k_x^{2n} \right)^2 + (vk_y)^2} \quad (10)$$

corresponds to the energy of the quasiparticles and $0 \leq \phi \leq \pi$, since $k_x^{2n} \geq 0$. Computing the Jacobian determinant, the element of area is:

$$d^2\mathbf{k} = \frac{2^{\frac{1}{2n}-1}}{nvg_n^{\frac{1}{2n}}} \varepsilon^{\frac{1}{2n}} (\sin \phi)^{\frac{1}{2n}-1} d\varepsilon d\phi. \quad (11)$$

Every two points in k -space are mapped to a single point in the (ε, ϕ) space as defined, and so one must add an additional factor of 2 to fully integrate over k -space in the new variables. It is useful to introduce a dimensionless energy variable

$$E = \left(\frac{g_n}{2\varepsilon}\right)^{\frac{1}{n}} \frac{\varepsilon^2}{v^2} = \left(\frac{\varepsilon}{q_n v}\right)^{2-\frac{1}{n}}, \quad (12)$$

where $q_n = (2v/g_n)^{\frac{1}{2n-1}}$ has units of momentum. In the new variables, the integral becomes:

$$\Sigma_y(\mathbf{p}) = vp_y \frac{\alpha}{4\pi} \int dE \int_0^\pi d\phi f(E, \phi), \quad (13)$$

where $\alpha = e^2/v$ is the dimensionless coupling constant and

$$f(E, \phi) = \frac{\cos^2 \phi}{(\sin \phi)^{1-(1/2n)} (\sin^{1/n} \phi + E \cos^2 \phi)^{3/2}}. \quad (14)$$

The integral sharply accumulates around $\phi = 0$ so we estimate:

$$\int_0^\pi d\phi f(E, \phi) \approx 2 \left(\int_0^a \frac{d\phi}{\phi^{1-(1/2n)} [\phi^{1/n} + E]^{3/2}} + \int_a^{\pi/2} d\phi f(E, \phi) \right) \quad (15)$$

$$\begin{aligned} &\approx 2 \int_0^a \frac{d\phi}{\phi^{1-(1/2n)} [\phi^{1/n} + E]^{3/2}} \\ &= \frac{4na^{1/2n}}{E\sqrt{a^{1/n} + E}}, \end{aligned} \quad (16)$$

for some a . We neglect the second term in Eq. (15) since it is finite as $E \rightarrow 0$. Taking $E \ll a^{1/n} \ll 1$ gives

$$\int_0^\pi d\phi f(E, \phi) \underset{E \rightarrow 0}{\approx} \frac{4n}{E}, \quad (17)$$

and thus

$$\Sigma_y(\mathbf{p}) = vp_y \frac{\alpha}{\pi} \frac{n}{2n-1} \int_{E_{\omega_{\mathbf{p}}}}^{E_\Lambda} dE \frac{1}{E} = vp_y \frac{\alpha}{\pi} \ln \left(\frac{\Lambda}{\omega_{\mathbf{p}}} \right). \quad (18)$$

As usual, we introduce a high energy cutoff Λ and integrate above an on-shell infrared energy cut-off $\omega_{\mathbf{p}} \equiv \varepsilon$, i.e. $E_{\omega_{\mathbf{p}}} < E < E_\Lambda$. The effective perturbative parameter that controls the expansion is $\bar{\alpha} \equiv \alpha/\pi < 1$, with $\alpha = e^2/v$ the dimensionless fine structure constant of the material.

B. Self-energy correction to g_n

To find the correction to g_n , we expand

$$V(\mathbf{k} - \mathbf{p}) = \frac{2\pi e^2}{|\mathbf{k} - \mathbf{p}|} = 2\pi e^2 \sum_{l=0}^{\infty} \frac{p^l}{k^{l+1}} P_l(\cos \gamma), \quad (19)$$

where P_l are the Legendre polynomials and $\cos \gamma = \frac{\mathbf{k} \cdot \mathbf{p}}{kp}$. The expansion is only valid for $k > p$, and only $l = \text{even}$ terms contribute to the integral in Eq. (7). We consider the term proportional to p_x^{2n} ($l = 2n$), and recast into the energy-angle coordinates in Eqs.(9),(12) to arrive at

$$\Sigma_x(\mathbf{p}) = \frac{g_n}{2} p_x^{2n} \frac{\alpha}{4\pi(2n-1)} \int \frac{dE}{E} \int d\phi L(E, \phi), \quad (20)$$

where

$$L(E, \phi) = \frac{\sin^{\frac{1}{2n}} \phi}{\left(\sin^{1/n} \phi + E \cos^2 \phi\right)^{n+\frac{1}{2}}} P_{2n}(\cos \gamma), \quad (21)$$

with

$$\cos \gamma = \frac{\sin^{1/2n} \phi (\cos \beta) + \sqrt{E} \cos \phi (\sin \beta)}{\sqrt{\sin^{1/n} \phi + E \cos^2 \phi}}. \quad (22)$$

and β is the polar angle of \mathbf{p} . Since the leading divergence occurs as $E \rightarrow 0$, we restrict the integral to

$$E \ll \frac{\sin^{1/n} \phi}{\cos^2 \phi}, \quad (23)$$

allowing us to approximate $\cos \gamma \approx \cos \beta = 1$, where we take \mathbf{p} to be along the x direction, and $L(E, \phi) \approx 1/\sin \phi$. The singularity is captured at small ϕ so we consider $E^n \ll \phi \ll 1$, where

$$\int_0^{\pi/2} d\phi L(E, \phi) \approx \int_{E^n} d\phi \frac{1}{\phi}, \quad (24)$$

and ignore the finite behavior on the upper bound. Neglecting subleading terms, we are left with

$$\int_{E_\omega}^{E_\Lambda} dE \frac{-2n \ln E}{E} = n \ln^2 \left(\frac{E_\Lambda}{E_\omega} \right), \quad (25)$$

finally yielding:

$$\Sigma_x(\mathbf{p}) = \frac{g_n}{2} p_x^{2n} \frac{\alpha}{4\pi} \frac{2n-1}{n} \ln^2 \left(\frac{\Lambda}{\omega_{\mathbf{p}}} \right). \quad (26)$$

This unconventional log squared singularity originally reported in semi-Dirac fermions ($n = 1$) appears for all n . This has a significant effect on the forthcoming RG analysis of this problem.

III. RENORMALIZATION GROUP

We set up the renormalization group (RG) equations

$$\frac{dg}{d\ell} = \frac{1}{2\pi} \frac{2n-1}{n} \alpha(\ell) g(\ell) \ell \quad (27)$$

$$\frac{dv}{d\ell} = \frac{1}{\pi} \alpha(\ell) v(\ell), \quad (28)$$

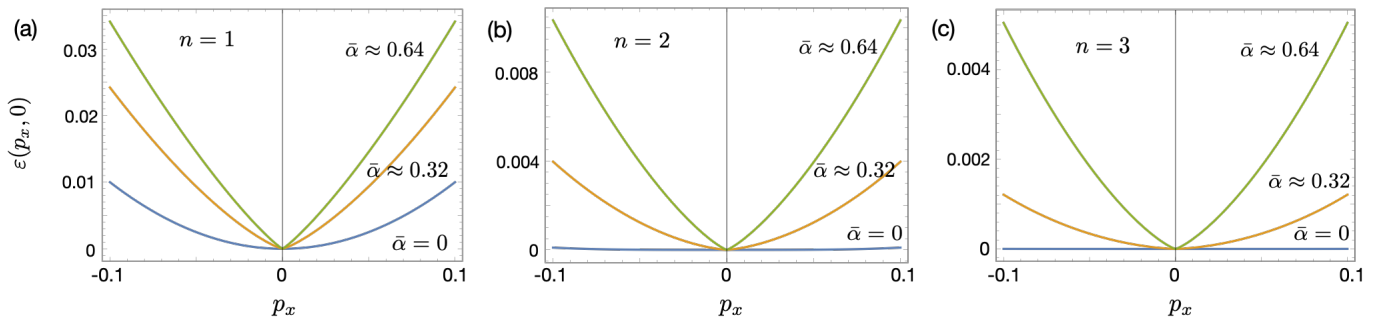


FIG. 3. Renormalized energy spectrum along the p_x direction for a) $n = 1$, b) $n = 2$ and c) $n = 3$. Energy ε and momentum p_x normalized by the ultraviolet cut-offs Λ and $p_\Lambda^x = (2\Lambda/g_0)^{1/2n}$ respectively. Blue lines describe the non-interacting spectrum of generalized semi-Dirac fermions, with $\propto p_x^{2n}$ dispersion. Orange lines correspond to the perturbative parameter $\bar{\alpha} \equiv \alpha_0/\pi \approx 0.32$ and green lines to $\bar{\alpha} \approx 0.64$. Interactions restore the linearity of the energy spectrum along the p_x direction in momentum for any integer $n \geq 1$. The effective velocity of the quasiparticles v_x in the renormalized spectrum has a weak dependence on n (see text).

where we introduce the RG scale $\ell = \ln \frac{\Lambda}{\omega_p}$. Since the charge does not renormalize, the solution to Eq.(28) is trivial, decoupling the equations. There are no higher order logs to sum for v , and α only renormalizes via its dependence on v . The solution to Eq.(27) reads

$$\frac{g(\omega)}{g_0} = \left[\frac{\Lambda/\omega}{\left(1 + \frac{\alpha_0}{\pi} \ln \frac{\Lambda}{\omega}\right)^{\pi/\alpha_0}} \right]^{\frac{2n-1}{2n}}, \quad (29)$$

with g_0 and α_0 as the bare constants. The strong power law dependence on ω has a profound effect on the spectrum. To see this more clearly we consider the renormalized dispersion along the two directions

$$\varepsilon(p_x, 0) = \frac{\Lambda}{p_\Lambda^x} \frac{1}{\left[1 + \frac{\alpha_0}{\pi} 2n \ln \left(\frac{p_\Lambda^x}{|p_x|}\right)\right]^{\frac{\pi}{\alpha_0} \frac{2n-1}{2n}}} |p_x| \quad (30)$$

$$\varepsilon(0, p_y) = v_0 \left[1 + \frac{\alpha_0}{\pi} \ln \left(\frac{\Lambda}{v_0 |p_y|}\right)\right] |p_y|, \quad (31)$$

where we define the characteristic high-energy momentum scale

$$p_\Lambda^x = \left(\frac{2\Lambda}{g_0}\right)^{1/2n}. \quad (32)$$

Remarkably, the resummation of log squared divergences to all orders of perturbation theory has produced a linear spectrum with a weak additional logarithmic correction. Note that this behavior is general for any $n \geq 1$, implying that interactions always drive the system towards linearity regardless of how flat the bare spectrum is. The dependence on n is quite weak, further exhibiting the universality of our result. Our results agree with those in Ref. [17] for the case of ordinary ($n = 1$) semi-Dirac fermions.

In Fig. 3 we plot the renormalization of the energy spectrum along the p_x direction for $\alpha_0/\pi \approx 0, 0.32$ and

0.64. Panel a) shows the renormalized energy spectrum (orange and green lines) for $n = 1$, in the conventional case of semi-Dirac fermions. As found before, the parabolic dispersion near the touching point becomes linear (up to weak logarithmic corrections to scaling) over a sizable energy range. This effect is even more pronounced for anisotropic bands that are flatter along the p_x direction in the vicinity of the neutrality point, as shown in panels b) and c), for $n = 2$ and 3 respectively. The effective renormalized velocity of the quasiparticles along that direction $v_x = \partial_{p_x} \varepsilon(p_x, 0)$, to leading order, has a weak dependence on n at finite momentum $p_x \ll p_\Lambda^x$. In other words, $v_x(\ell)$ is weakly dependent on the form of the original free dispersion. This is a non-trivial, non-perturbative effect that results from the resummation of leading logs to all powers in perturbation theory in the RG flow, even though the system is still within the perturbative regime $\alpha_0/\pi < 1$. As we discuss below, as $\alpha_0/\pi \rightarrow 0$, the energy window where the restoration of linearity occurs becomes exponentially small compared to the ultraviolet cut-off Λ . For typical finite values $\alpha_0/\pi < 1$, the energy window can be fairly wide and is amenable to experimental observation. This is to be contrasted with resummations typically encountered in non-perturbative $1/N_f$ expansions, which result in finite corrections to the dynamical critical exponents that scale to leading order with $1/N_f$ [15, 25–27].

IV. ULTRA-LOW ENERGY REGIME

Because the bare density of states vanishes near the neutrality point with sublinear power law dependence in momentum along the k_y direction, the Coulomb interaction diverges faster with momentum in the infrared. This requires us to consider the effects of long-distance screening on the self-energy. The static polarization function $\Pi(\mathbf{k}, \nu = 0)$ along the two axes (diagrammatically shown

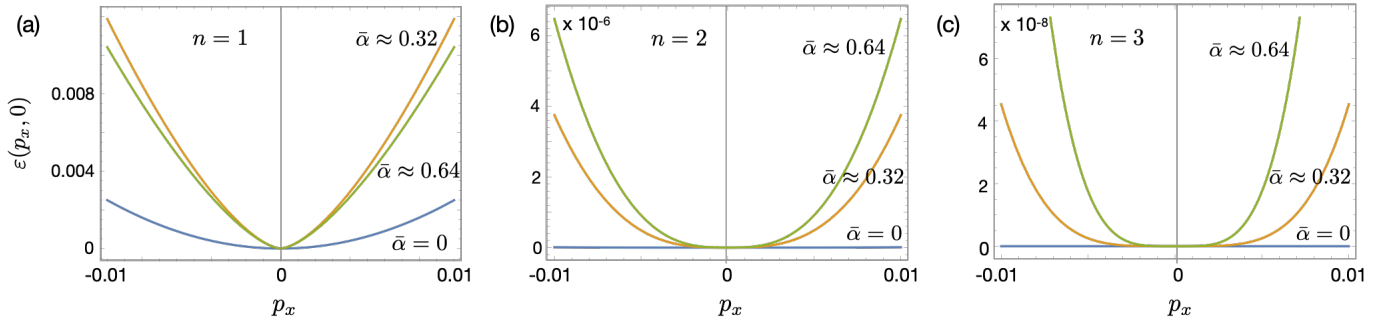


FIG. 4. Renormalized energy spectrum along the p_x direction in the RPA dominated, ultra-low energy regime ($N_f = 1$) for a) $n = 1$, b) $n = 2$, and c) $n = 3$. Energy ε and momentum p_x normalized by the ultraviolet cut-offs Λ and $p_\Lambda^x = (2\Lambda/g_0)^{1/2n}$ respectively. Blue lines: $\bar{\alpha} = 0$; orange lines: $\bar{\alpha} \equiv \alpha/\pi \approx 0.32$; green lines: $\bar{\alpha} \approx 0.64$. In this regime interactions produce weaker corrections to the energy spectrum. The peculiar non-monotonic dependence of g_n on α is clearly visible in panel a) (see text).

in Fig. 2b) can be calculated analytically to give:

$$\Pi(k_x, 0) = -\frac{|k_x|}{4\pi^2 v} a_n \quad (33)$$

$$\Pi(0, k_y) = -\frac{\left(\frac{2v}{g_n}\right)^{\frac{1}{2n}} |k_y|^{\frac{1}{2n}}}{2\pi v} c_n, \quad (34)$$

where

$$a_n = \int_{-\infty}^{\infty} dx \left[1 - \frac{x^{2n}(x+1)^{2n}}{(x+1)^{4n} - x^{4n}} 4n \ln\left(\frac{x+1}{x}\right) \right] \quad (35)$$

and

$$c_n = \frac{\Gamma\left(1 + \frac{1}{4n}\right) \sqrt{\pi} \csc\left(\frac{\pi}{4n}\right)}{\Gamma\left(\frac{3}{2} + \frac{1}{4n}\right) 2^{2+1/2n} n}. \quad (36)$$

The integral in Eq.(35) can be exactly evaluated for $n = 1$; $a_1 = \pi^2/4 \approx 2.47$, whereas $c_1 = \sqrt{\pi} \Gamma(\frac{5}{4})/\Gamma(\frac{7}{4}) \approx 0.44$. For the other relevant cases ($n = 2, 3$), $a_2 \approx 5.36$, $a_3 \approx 8.19$, $c_2 \approx 0.30$ and $c_3 \approx 0.22$.

The polarization bubble has linear in momentum scaling along the k_x direction and sublinear momentum dependence along the k_y direction. Calculating the self-energy corrections under the dressed Coulomb interaction $V_{\text{RPA}}(\mathbf{k}) = V(\mathbf{k})/[1 - V(\mathbf{k})\Pi(\mathbf{k})]$, as we show in more detail in Appendix A, we replace the bare Coulomb propagator with the screened one. The integral appearing in Eq. (25) is replaced with

$$\int_{E_\omega}^{E_\Lambda} dE \frac{\ln\left(\sqrt{E} + c_n \alpha N_f\right)}{E}, \quad (37)$$

where N_f is the number of fermionic species. In the ultra-low energy regime $\sqrt{E} \ll c_n \alpha N_f$, or equivalently for

$$\varepsilon \ll v q_n (c_n \alpha N_f)^{\frac{2n}{2n-1}}, \quad (38)$$

screening precludes the emergence of a log square term.

In this regime, the corrections are:

$$v \rightarrow v \left[1 + \frac{\alpha}{2\pi n} \ln\left(\frac{\Lambda}{\omega_{\mathbf{p}}}\right) \right] \quad (39)$$

$$g_n \rightarrow g_n \left[1 + \frac{\alpha}{\pi} \ln\left(\frac{1}{\alpha'}\right) \ln\left(\frac{\Lambda}{\omega_{\mathbf{p}}}\right) \right] \quad (40)$$

The correction to v has now acquired an n dependent coefficient. More importantly, the RPA screening has ‘split’ the log square, leaving a single log divergence with a non-perturbative coefficient. Note that this has been studied in detail for the $n = 1$ case in Ref. [15], where they calculate the log coefficients to be twice what we find. Nevertheless, it is the ratio of coefficients that determines the RG flow and hence the forthcoming results are in exact agreement with their work near the fixed point of the problem.

We proceed as in Section III, and find that again the velocity does not run in the ultra-low energy regime, whereas

$$\frac{g(\ell)}{g_0} = \left(1 + \frac{\alpha_0}{2\pi n} \ell\right)^{\gamma_n(\ell)}, \quad (41)$$

with the exponent

$$\gamma_n(\ell) = n \ln \left[\frac{1 + \frac{\alpha_0}{2\pi n} \ell}{(c_n \alpha_0 N_f)^2} \right]. \quad (42)$$

The correction to g has lost the power law in ω , but has acquired a particularly strong logarithmic correction. The effect is much more sensitive to the value of n , and less sensitive to the value of α_0 . There is no general behavior for all n , but the spectrum is still significantly enhanced:

$$\varepsilon(p_x, 0) = \frac{g_0}{2} \left(1 + \frac{\alpha_0}{2\pi n} \ell\right)^{\gamma_n(\ell)} p_x^{2n} \quad (43)$$

$$\varepsilon(0, p_y) = v_0 \left[1 + \frac{\alpha_0}{2\pi n} \ln\left(\frac{\Lambda}{v_0 |p_y|}\right) \right] |p_y|. \quad (44)$$

The effect is suppressed in the y direction with increasing n , but in the x direction the behavior is more subtle, and

is determined by the interplay between α_0 , n , and N_f . We show the renormalized energy spectrum along the p_x direction for the ultra-low energy regime in the three panels of Fig. 4 for $n = 1, 2$ and 3 . For fixed n, N_f , and p_x , the spectrum is enhanced up to a critical value of α_0 (approximately $\alpha_0 \approx n/N_f$), then begins to saturate as α_0 increases further. This can be seen clearly in Fig. 4a), for $n = 1, N_f = 1$ where the maximally enhanced spectrum occurs at $\bar{\alpha}_0 \equiv \alpha_0/\pi \approx 0.3$.

As the RG flows towards the non-interacting fixed point of the theory at $\alpha \rightarrow 0$, the linearity of the energy spectrum is restored for

$$\varepsilon \lesssim \Lambda e^{-\sqrt{\frac{n}{2n-1}}\pi/\alpha}, \quad (45)$$

setting an upper bound on energy past which $\frac{\alpha}{\pi} \frac{2n-1}{n} \ln^2\left(\frac{\Lambda}{\omega}\right) \lesssim 1$, and the RG resummation is not justified. Therefore the region $\varepsilon > \Lambda e^{-\sqrt{\frac{n}{2n-1}}\pi/\alpha}$ corresponds to the high-energy free fermion regime, where the spectrum is unrenormalized. The restoration of linearity of the spectrum persists all the way down to a second energy scale, where screening effects become dominant. This low energy scale is set by Eq. (38),

$$\varepsilon_n = vq_n(c_n\alpha N_f)^{\frac{2n}{2n-1}}. \quad (46)$$

Below $\varepsilon \lesssim \varepsilon_n$, the system is in the ultra-low energy RPA dominated regime.

This behavior is illustrated in Fig. 5, where the different weak coupling regimes of the RG flow are shown. The dark blue area corresponds to the high-energy, free fermion regime, followed by an intermediate regime (light green) with restoration of linearity in the spectrum. The deep infrared RPA dominated regime is shown in yellow. In this regime, screened Coulomb interactions produce a logarithmic renormalization to the energy spectrum.

In panel 5b) we quantitatively show the boundaries between the different regimes for $n = 1$ and $N_f = 4$ as a function of the perturbative coupling $\alpha/\pi < 1$. The boundaries are weakly dependent on n and retain the same qualitative features for $n = 2, 3$ as in the $n = 1$ case. For N of order 1, the energy window of the linear spectrum regime is wide at finite coupling α/π and persists all the way down to the weak coupling $\alpha \rightarrow 0$ limit, although it becomes exponentially small. The lower bound of the linear regime, ε_n , increases with the fermionic degeneracy N_f as $\varepsilon_n \propto N_f^{\frac{2n}{2n-1}}$, raising the slope of the curve that delimits the RPA region from above (yellow region). In the large N_f limit, considered in Ref. [15] for the $n = 1$ case, the RPA region takes over the linear spectrum regime, and a non-perturbative analysis of the problem is required. For finite N_f , and in specific for N_f of order 1, restoration of the linearity of the spectrum is present over a significant energy range in units of the ultraviolet cut-off Λ . We discuss our results in light of the existing literature in Section VI.

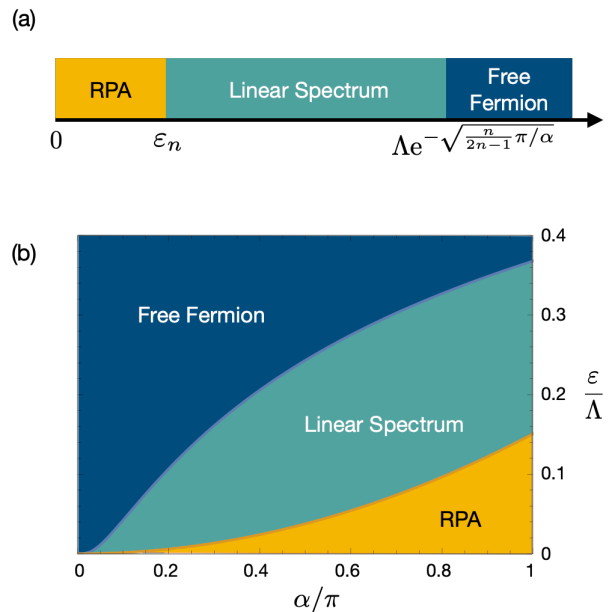


FIG. 5. Different weak coupling regimes in the RG flow for generalized semi-Dirac fermions. a) The electrons are unrenormalized (free fermion) at high energies (dark blue region). In the intermediate regime (light green) $\varepsilon_n \lesssim \varepsilon \lesssim \Lambda e^{-\sqrt{\frac{n}{2n-1}}\pi/\alpha}$, resummation of log square divergences leads to the restoration of the linearity in the spectrum, regardless of the strength of the coupling $\alpha/\pi \lesssim 1$ or the flatness of the bands (indicated by n). The yellow area indicates the ultra-low energy regime $\varepsilon \ll \varepsilon_n \sim vq_n(\alpha N_f)^{2n/(2n-1)}$ (see text), where RPA screening is dominant. In this regime, interactions produce a particularly strong logarithmic renormalization of the spectrum, but do not reduce the power law. b) Plot of the boundaries between different regimes versus the perturbative coupling α/π for $n = 1$ and $N_f = 4$. The boundaries are weakly dependent on n and have a qualitatively similar shape for $n = 2$ and 3 . The energy window of the regime with linear spectrum is suppressed in the non-interacting limit $\alpha \rightarrow 0$, but extends over a wide energy range for finite coupling $\alpha/\pi < 1$. The lower bound of the window increases with the number of fermionic species N_f as $\propto N_f^{2n/(2n-1)}$. The RPA dominated regime takes over the intermediate linear spectrum regime in the large N_f limit, but remains subdominant to the linear spectrum regime when N_f is of order 1 over a wide range of energies.

V. PHYSICAL OBSERVABLES

A. Density of States

We now calculate the density of states

$$\rho(\omega) = \frac{1}{(2\pi)^2} \int d^2\mathbf{k} \delta(\omega - \varepsilon(\mathbf{k})) \quad (47)$$

for the renormalized spectra in the three regimes shown in Fig. 5. We approximate that the logarithmic corrections are slowly-varying functions and thus may be considered constant over the integral. However, we re-

tain the strong power law correction in the case of the long-range interaction. This yields an anisotropic Dirac cone with an effective velocity in the x direction,

$$v_x(\ell) = \frac{\Lambda}{p_\Lambda^x} \left(1 + \frac{\alpha_0}{\pi} \ell\right)^{-\frac{\pi}{\alpha_0} \frac{2n-1}{2n}}, \quad (48)$$

This velocity is affected by weak logarithmic corrections, $\ell = \ln(\Lambda/\omega)$. The resulting density of states as a function of energy is:

$$\rho(\omega) = \frac{p_\Lambda^x}{2\pi v_0} \frac{\omega}{\Lambda} \left[1 + \frac{\alpha_0}{\pi} \ln\left(\frac{\Lambda}{\omega}\right)\right]^{\left(\frac{2n-1}{2n}\right) \frac{\pi}{\alpha_0} - 1}, \quad (49)$$

recovering the linearity of the DOS for conventional Dirac fermions.

In the ultra-low energy regime, where interactions are partially screened by polarization effects, $g(\omega)$ does not have a power law dependence. Hence we simply calculate the density of states for the free model and restore the logarithmic corrections after the integral is evaluated. The result is

$$\rho(\omega) = \frac{1}{(2\pi)^2 v_0} \left(\frac{2}{g_0}\right)^{\frac{1}{2n}} \omega^{\frac{1}{2n}} \frac{d_n}{n} \left[1 + \frac{\alpha_0}{2\pi n} \ln\left(\frac{\Lambda}{\omega}\right)\right]^{-\delta_n(\omega)} \quad (50)$$

where

$$\delta_n(\omega) = 1 + \frac{1}{2} \ln \left[\frac{1 + \frac{\alpha_0}{2\pi n} \ln\left(\frac{\Lambda}{\omega}\right)}{(c_n \alpha_0 N_f)^2} \right], \quad (51)$$

and

$$d_n = \frac{1}{2^{1-1/2n} \Gamma\left(\frac{1}{2n}\right)} \left(\frac{\pi \csc\left(\frac{\pi}{4n}\right)}{\Gamma\left(1 - \frac{1}{4n}\right)} \right)^2. \quad (52)$$

Note that taking the limit $\alpha_0/\pi \rightarrow 0$ in both expressions recovers the correct $\omega^{1/2n}$ dependence for the free density of states, but the coefficients do not agree. The RG flow to linearity has significantly reduced the anisotropy in the system, producing a coefficient independent of n . In the screening regime, angular integrals generate the dependence d_n/n .

The effect of the renormalization of the energy spectrum in the DOS is shown in Fig. 6. The non-interacting DOS for $n = 1, 2, 3$ is shown in the blue curves, where $\rho \propto \varepsilon^{\frac{1}{2n}}$. Orange and green curves correspond to $\alpha/\pi \approx 0.32$ and 0.64 respectively. On the left column, we show the renormalized DOS in the intermediate linear regime, where the DOS scales linearly with ε up to logarithmic corrections to scaling. On the right column, we show the DOS in the ultra-low energy regime, where the DOS has modest logarithmic corrections that are consistent with marginal Fermi liquid behavior.

B. Heat Capacity

The heat capacity is defined as $C_V = -T\partial^2 F/\partial T^2$, where F is the thermodynamic free energy and we calcu-

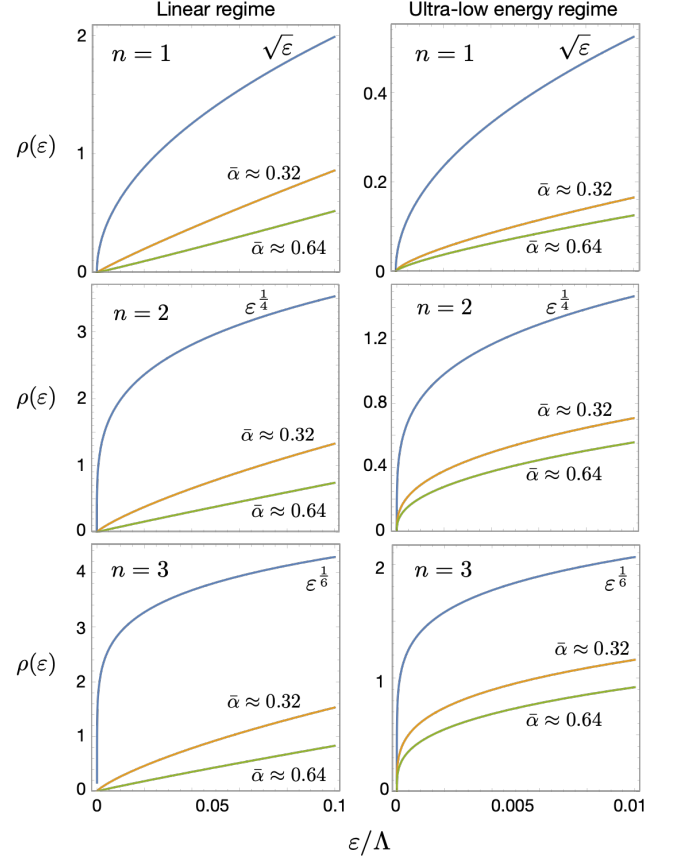


FIG. 6. Density of states vs energy ε in the perturbative linear regime (left column) and in the ultra-low energy regime (right column) for $n = 1$ (top panels) $n = 2$ (middle) and $n = 3$ (bottom). Blue lines: bare energy spectrum for generalized semi-Dirac fermions, with $\rho \propto \varepsilon^{1/2n}$. Orange: $\bar{\alpha} \approx 0.32$; green $\bar{\alpha} \approx 0.64$. Under the bare Coulomb interaction, the crossover from $\propto \varepsilon^{1/2n}$ to a linear dependence on energy occurs quickly as interactions are turned on. In the RPA dominated ultra-low energy regime, increasing interaction strength is less impactful, and particularly so for increasing n . This is partly due to the $1/n$ factor incurred in Σ_y . The density of states has units of $p_\Lambda^x/2\pi v_0$ and $p_\Lambda^x/(2\pi)^2 v_0$ in the left and right columns respectively, and energy is normalized by the ultraviolet cut-off Λ .

late it via

$$C_V(T) = \frac{1}{(2\pi)^2} \frac{1}{T^2} \int d^2\mathbf{k} \left(\frac{\varepsilon(\mathbf{k})}{\cosh[\varepsilon(\mathbf{k})/2T]} \right)^2. \quad (53)$$

Adopting the same approach as in subsection V A, we find the heat capacity in the unscreened case to be

$$C_V(T) = \frac{\zeta(3)}{9\pi} \frac{p_\Lambda^x}{v_0 \Lambda} T^2 \left[1 + \frac{\alpha_0}{\pi} \ln\left(\frac{\Lambda}{T}\right)\right]^{\left(\frac{2n-1}{2n}\right) \frac{\pi}{\alpha_0} - 1} \quad (54)$$

where ζ is the Riemann-zeta function. Whereas the unrenormalized heat capacitance for generalized semi-Dirac fermions scales as $C_V \sim T^{1+\frac{1}{2n}}$, restoration of linearity

in the spectrum recovers the usual dependence for Dirac fermions, $C_V \sim T^2$, up to weak logarithmic corrections.

In the ultra-low energy regime, the heat capacity changes to

$$C_V(T) = \frac{(2/g_0)^{1/2n}}{(2\pi)^2 v_0} T^{1+\frac{1}{2n}} \frac{d_n}{n} b_n \left[1 + \frac{\alpha_0}{2\pi n} \ln \left(\frac{\Lambda}{T} \right) \right]^{-\nu_n(T)} \quad (55)$$

where

$$\nu_n(T) = 1 + \frac{1}{2} \ln \left[\frac{1 + \frac{\alpha_0}{2\pi n} \ln \left(\frac{\Lambda}{T} \right)}{(c_n \alpha_0 N_f)^2} \right], \quad (56)$$

and

$$b_n = \int_0^\infty dx \frac{x^{2+\frac{1}{2n}}}{(\cosh \frac{x}{2})^2}, \quad (57)$$

where $b_1 \approx 11.53$, $b_2 \approx 8.63$ and $b_3 \approx 7.87$.

C. Landau Levels

Finally, we consider the behavior in a strong transverse magnetic field B by applying the semiclassical quantization condition $S(\varepsilon) = 2\pi(N + \frac{1}{2})eB$, where $S(\varepsilon) = (2\pi)^2 \int_0^\varepsilon d\omega \rho(\omega)$ is the area enclosed by a constant energy contour in momentum space for the zero-field spectrum [28]. The semiclassical approximation has been checked against an exact numerical solution for the case $n = 1$, and has been found to be in excellent agreement [1]. Note that the relative phase of $1/2$ cannot be obtained from semiclassical arguments, and arises as a consequence of the zero Berry phase around the semi-Dirac point. The resultant energy spectrum of Landau levels for non-interacting generalized semi-Dirac fermions is

$$\varepsilon_N = \pm \left[v \left(\frac{g_n}{2} \right)^{\frac{1}{2n}} \frac{2n+1}{2d_n} 2\pi \left(N + \frac{1}{2} \right) eB \right]^{\frac{2n}{2n+1}}, \quad (58)$$

with $N \in \mathbb{N}$. Renormalization of the Landau levels in the linear regime recovers the $\sqrt{v_x(\ell)v_y(\ell)B}$ scaling for anisotropic Dirac fermions with effective velocity $v_x(\ell)$ and $v \rightarrow v(\ell) \equiv v_y(\ell)$ as in Section III. In the ultra-low energy regime, we simply renormalize the parameters in Eq.(58) to $g_n \rightarrow g_n(\ell)$, $v \rightarrow v(\ell)$ as in Section IV. In the presence of a magnetic field, ω in $\ell = \ln(\Lambda/\omega)$ is bounded from below by an infrared energy cutoff on the order of the spacing between Landau levels.

VI. CONCLUSIONS

In summary, we examined the many-body renormalization of generalized semi-Dirac fermions, which disperse linearly in one direction and have nearly flat bands near the neutrality point in the perpendicular direction with momentum dependence $\propto p_x^{2n}$. For larger values of $n > 1$

the spectrum becomes increasingly flat around the touching points of the bands. We showed that the regime with restoration of linearity of the spectrum along the p_x direction is present for arbitrary $n > 1$, and is observable over a relatively large energy window. This remarkable lifting of the semi-Dirac anisotropy for arbitrarily flat bands is a severe effect driven by long-range interactions.

Previous large N_f results identified essentially three different scaling regimes in the RG flow, as the dimensionless coupling α gets renormalized towards the weak coupling fixed point of the problem: a marginal Fermi liquid regime at very low energies, which coincides with the RPA regime we discussed for $n = 1$, a high energy, free fermion regime, and an intermediate non-Fermi liquid regime that emerges from the large N_f calculation. We point to the existence of a new regime with anisotropic linear dispersion that follows from the non-trivial resummation of leading log square divergences to all orders in perturbation theory. This phase takes precedence over the non-Fermi liquid regime of the large N_f calculation in the situation where $\alpha/\pi < 1$ and N_f is of order 1, when conventional perturbation theory applies. We showed this regime appears over a wide energy window and could be experimentally observed for instance for $n = 1$. As N_f becomes large, the energy window progressively shrinks as the lower bound for the linear spectrum regime grows.

As for the realization of generalized semi-Dirac fermions with $n > 1$, we argue that it is theoretically possible in the following way. When two Dirac cones merge in a tight binding lattice model, the linear term in the low energy expansion vanishes along one direction and the leading term is quadratic in momentum, where the effective mass is a sum over hoppings and lattice vectors [2]. If the underlying lattice geometry and hoppings are such that this sum vanishes, then the leading behavior becomes $\propto p_x^4$, realizing the $n = 2$ case in this class of Hamiltonians, and so forth. Depending on the microscopic model and the symmetry group of the lattice, this cancellation can be possible in principle. Finally, we mention that the diagram in Fig. 2a) also generates lower-power even terms, not originally present in the Hamiltonian, i.e. for the case $n = 2$, a term $\propto t p_x^2 \sigma_x$ appears, with t being a non-universal, cutoff dependent constant. Such terms, naturally, do not affect our RG analysis and the conclusions of the present work.

The signature features of the many-body effects we describe can be observed in angle-resolved photoemission experiments [29], which can probe the renormalization of the quasiparticle energy spectrum; and also in quantum capacitance measurements of the electronic compressibility [30, 31], which can probe the temperature dependence of the heat capacitance. Moreover, the signature $B^{2n/2n+1}$ scaling of the Landau levels can be detected via magneto-optical spectroscopy techniques, as presented in Ref.[32] for the nodal line semimetal ZrSiS.

ACKNOWLEDGMENTS

We would like to thank A. Chubukov for enlightening discussions. BU acknowledges NSF grant No DMR-2024864 for support. MME and VNK gratefully acknowledge the financial support from NASA Grant No. 80NSSC19M0143, and the CEMS Summer Graduate Fellowship at the University of Vermont.

Appendix A: Screened interactions

We use an ansatz for the static polarization bubble for generalized semi-Dirac fermions that recovers the exact results along the two directions:

$$\Pi(k_x, k_y) = - \left[(f_n)^{4n} k_x^{4n} + (h_n)^{4n} k_y^{4n} \right]^{\frac{1}{4n}}, \quad (\text{A1})$$

where

$$f_n = \frac{1}{4\pi^2 v} a_n, \quad h_n = \frac{1}{2\pi v} \left(\frac{2v}{g_n} \right)^{\frac{1}{2n}} c_n, \quad (\text{A2})$$

with a_n and c_n dimensionless constants defined in Eq. (35) and (36). Using the parametrization (9),

$$\frac{g_n}{2} k_x^{2n} = \varepsilon \sin \phi, \quad v k_y = \varepsilon \cos \phi, \quad (\text{A3})$$

with $\phi \in [0, \pi]$, then $\Pi(\varepsilon, \phi) = - \left(\frac{2\varepsilon}{g_n} \right)^{\frac{1}{2n}} \pi_0(\phi)$, with

$$\pi_0(\phi) = \left[(f_n)^{4n} \sin^2 \phi + (h_n')^{4n} \cos^2 \phi \right]^{\frac{1}{4n}}, \quad (\text{A4})$$

where $h_n' = c_n/(2\pi v)$. The screened Coulomb interaction becomes

$$\begin{aligned} V_{\text{RPA}}(\mathbf{k}) &= \frac{2\pi e^2}{|\mathbf{k}| - 2\pi v \alpha N_f \Pi(\mathbf{k})} \\ &= \frac{2\pi e^2 \left(\frac{g_n}{2\varepsilon} \right)^{\frac{1}{2n}}}{\left[\sqrt{\sin^{\frac{1}{n}} \phi + E \cos^2 \phi + 2\pi v \alpha N_f \pi_0(\phi)} \right]}, \end{aligned} \quad (\text{A5})$$

where $E = [\varepsilon/(q_n v)]^{2-1/n}$ is dimensionless, and $q_n = (2v/g_n)^{\frac{1}{2n-1}}$ has units of momentum. Expanding Σ_x in Eq.(7) for small external \mathbf{p} and transforming momentum

integration variables to (ε, ϕ) coordinates, we find that the term

$$\frac{h_x(\mathbf{k} + \mathbf{p})}{\sqrt{h_x^2(\mathbf{k} + \mathbf{p}) + h_y^2(\mathbf{k} + \mathbf{p})}} \approx \frac{g_n}{2} p_x^{2n} \frac{\cos^{4n} \phi}{\varepsilon} \quad (\text{A6})$$

produces the most singular contribution to the integral.

Hence,

$$\begin{aligned} \Sigma_x(\mathbf{p}) &= \frac{g_n}{2} p_x^2 \frac{\alpha}{4\pi} \frac{1}{2n-1} \int_{E_\omega}^{E_\Lambda} \frac{dE}{E} \int_0^\pi d\phi \frac{\cos^{4n} \phi}{(\sin \phi)^{\frac{2n-1}{2n}}} \\ &\quad \times \frac{1}{\left[\sqrt{\sin^{\frac{1}{n}} \phi + E \cos^2 \phi + 2\pi v \alpha N_f \pi_0(\phi)} \right]}. \end{aligned} \quad (\text{A7})$$

The dominant contribution in the integrand occurs for small ϕ in the limit of $E \rightarrow 0$, ($E^n \ll \phi$). Approximating $\sin \phi \sim \phi$, $\cos \phi \sim 1$ the integral in ϕ becomes

$$2 \int_{E^n}^{\pi/2} d\phi \frac{1}{\phi^{\frac{2n-1}{2n}}} \frac{1}{\phi^{\frac{1}{2n}} + 2\pi v \alpha N_f h_n'} = -2n \ln \left(\sqrt{E} + \alpha' \right). \quad (\text{A8})$$

up to a constant, and $\alpha' = \alpha N_f c_n$. Hence, in the ultra-low energy regime, where $\sqrt{E} \ll \alpha'$,

$$\begin{aligned} \Sigma_x(\mathbf{p}) &= \frac{g_n}{2} p_x^2 \frac{\alpha}{4\pi} \frac{-4n}{2n-1} \int_{E_\omega}^{E_\Lambda} \frac{dE}{E} \ln \left(\sqrt{E} + \alpha' \right) \\ &\approx \frac{g_n}{2} p_x^2 \frac{\alpha}{\pi} \ln \left(\frac{1}{\alpha'} \right) \ln \left(\frac{\Lambda}{\omega} \right). \end{aligned} \quad (\text{A9})$$

To find the velocity correction Σ_y we expand $V_{\text{RPA}}(\mathbf{k} - \mathbf{p})$ to linear order in p_y similarly to Eq.(8). The term that generated the singularity for the bare interaction is now finite as $E \rightarrow 0$, and the leading divergence is now produced by

$$\begin{aligned} \Sigma_y &= v p_y \frac{\alpha}{4\pi} \frac{\alpha'}{2n(2n-1)} \int_{E_\omega}^{E_\Lambda} \frac{dE}{E} \int_0^\pi d\phi \frac{\cos^{1/2n} \phi}{(\sin \phi)^{\frac{2n-1}{2n}}} \\ &\quad \times \frac{1}{\left(\sqrt{\sin^{1/n} \phi + E \cos^2 \phi + \alpha' \cos^{1/2n} \phi} \right)^2} \end{aligned} \quad (\text{A10})$$

Approximating the ϕ integral in a similar fashion to Eq.(A8) we arrive at

$$\Sigma_y = v p_y \frac{\alpha}{4\pi} \frac{2\alpha'}{2n-1} \int_{E_\omega}^{E_\Lambda} \frac{dE}{E} \frac{1}{\sqrt{E} + \alpha'} \quad (\text{A11})$$

$$= v p_y \left(\frac{\alpha}{2\pi n} \ln \frac{\Lambda}{\omega} \right). \quad (\text{A12})$$

The effect of screening on the renormalization of v is much milder than the splitting of the log squared in Σ_x , but it does change the coefficient numerically and generates a $1/n$ dependence.

- [1] P. Dietl, F. Piéchon, and G. Montambaux, New magnetic field dependence of Landau levels in a graphenelike structure, *Physical review letters* **100**, 236405 (2008).
- [2] G. Montambaux, F. Piéchon, J.-N. Fuchs, and M. O. Goerbig, Merging of Dirac points in a two-dimensional crystal, *Physical Review B - Condensed Matter and Materials Physics* **80**, 153412 (2009).
- [3] J. Kim, S. S. Baik, S. H. Ryu, Y. Sohn, S. Park, B.-G. Park, J. Denlinger, Y. Yi, H. J. Choi, and K. S. Kim, Observation of tunable band gap and anisotropic Dirac semimetal state in black phosphorus, *Science* **349**, 723 (2015).
- [4] J. Kim, S. S. Baik, S. W. Jung, Y. Sohn, S. H. Ryu, H. J. Choi, B.-J. Yang, and K. S. Kim, Two-dimensional dirac fermions protected by space-time inversion symmetry in black phosphorus, *Physical review letters* **119**, 226801 (2017).
- [5] Y. Shao, A. Rudenko, J. Hu, Z. Sun, Y. Zhu, S. Moon, A. Millis, S. Yuan, A. Lichtenstein, D. Smirnov, *et al.*, Electronic correlations in nodal-line semimetals, *Nature Physics* **16**, 636 (2020).
- [6] B. Amorim, A. Cortijo, F. De Juan, A. G. Grushin, F. Guinea, A. Gutiérrez-Rubio, H. Ochoa, V. Parente, R. Roldán, P. San-Jose, *et al.*, Novel effects of strains in graphene and other two dimensional materials, *Physics Reports* **617**, 1 (2016).
- [7] S. Katayama, A. Kobayashi, and Y. Suzumura, Pressure-induced zero-gap semiconducting state in organic conductor α -(BEDT-TTF) 2I3 salt, *Journal of the Physical Society of Japan* **75**, 054705 (2006).
- [8] V. Pardo and W. E. Pickett, Half-metallic semi-Dirac-point generated by quantum confinement in TiO_2/VO_2 nanostructures, *Physical review letters* **102**, 166803 (2009).
- [9] H. Huang, Z. Liu, H. Zhang, W. Duan, and D. Vanderbilt, Emergence of a Chern-insulating state from a semi-Dirac dispersion, *Physical Review B* **92**, 161115 (2015).
- [10] B. Uchoa and K. Seo, Superconducting states for semi-Dirac fermions at zero and finite magnetic fields, *Physical Review B* **96**, 220503 (2017).
- [11] M. D. Uryszek, E. Christou, A. Jaefari, F. Krüger, and B. Uchoa, Quantum criticality of semi-Dirac fermions in $2+1$ dimensions, *Physical Review B* **100**, 155101 (2019).
- [12] M. D. Uryszek, F. Krüger, and E. Christou, Fermionic criticality of anisotropic nodal point semimetals away from the upper critical dimension: Exact exponents to leading order in $1/N_f$, *Physical Review Research* **2**, 043265 (2020).
- [13] B. Roy and M. S. Foster, Quantum multicriticality near the Dirac-semimetal to band-insulator critical point in two dimensions: A controlled ascent from one dimension, *Physical Review X* **8**, 011049 (2018).
- [14] V. N. Kotov, B. Uchoa, V. M. Pereira, F. Guinea, and A. Castro Neto, Electron-electron interactions in graphene: Current status and perspectives, *Reviews of modern physics* **84**, 1067 (2012).
- [15] H. Isobe, B.-J. Yang, A. Chubukov, J. Schmalian, and N. Nagaosa, Emergent non-fermi-liquid at the quantum critical point of a topological phase transition in two dimensions, *Physical review letters* **116**, 076803 (2016).
- [16] G. Y. Cho and E.-G. Moon, Novel quantum criticality in two dimensional topological phase transitions, *Scientific Reports* **6**, 19198 (2016).
- [17] V. N. Kotov, B. Uchoa, and O. P. Sushkov, Coulomb interactions and renormalization of semi-Dirac fermions near a topological Lifshitz transition, *Physical Review B* **103**, 045403 (2021).
- [18] Y. Cao, V. Fatemi, A. Demir, S. Fang, S. L. Tomarken, J. Y. Luo, J. D. Sanchez-Yamagishi, K. Watanabe, T. Taniguchi, E. Kaxiras, *et al.*, Correlated insulator behaviour at half-filling in magic-angle graphene superlattices, *Nature* **556**, 80 (2018).
- [19] Y. Cao, V. Fatemi, S. Fang, K. Watanabe, T. Taniguchi, E. Kaxiras, and P. Jarillo-Herrero, Unconventional superconductivity in magic-angle graphene superlattices, *Nature* **556**, 43 (2018).
- [20] X. Lu, P. Stepanov, W. Yang, M. Xie, M. A. Aamir, I. Das, C. Urgell, K. Watanabe, T. Taniguchi, G. Zhang, *et al.*, Superconductors, orbital magnets and correlated states in magic-angle bilayer graphene, *Nature* **574**, 653 (2019).
- [21] Y. Saito, J. Ge, K. Watanabe, T. Taniguchi, and A. F. Young, Independent superconductors and correlated insulators in twisted bilayer graphene, *Nature Physics* **16**, 926 (2020).
- [22] L. Wang, E.-M. Shih, A. Ghiotto, L. Xian, D. A. Rhodes, C. Tan, M. Claassen, D. M. Kennes, Y. Bai, B. Kim, *et al.*, Correlated electronic phases in twisted bilayer transition metal dichalcogenides, *Nature materials* **19**, 861 (2020).
- [23] Y. Quan and W. E. Pickett, A maximally particle-hole asymmetric spectrum emanating from a semi-Dirac point, *Journal of Physics: Condensed Matter* **30**, 075501 (2018).
- [24] J. Carbotte, K. Bryenton, and E. Nicol, Optical properties of a semi-Dirac material, *Physical Review B* **99**, 115406 (2019).
- [25] M. S. Foster and I. L. Aleiner, Graphene via large N: A renormalization group study, *Physical Review B—Condensed Matter and Materials Physics* **77**, 195413 (2008).
- [26] R. Nandkishore and L. Levitov, Electron interactions in bilayer graphene: Marginal Fermi liquid and zero-bias anomaly, *Physical Review B—Condensed Matter and Materials Physics* **82**, 115431 (2010).
- [27] X. Dou, A. Jaefari, Y. Barlas, and B. Uchoa, Quasiparticle renormalization in ABC graphene trilayers, *Physical Review B* **90**, 161411 (2014).
- [28] G. Montambaux, F. Piéchon, J.-N. Fuchs, and M. Goerbig, A universal Hamiltonian for motion and merging of Dirac points in a two-dimensional crystal, *The European Physical Journal B* **72**, 509 (2009).
- [29] A. Bostwick, T. Ohta, T. Seyller, K. Horn, and E. Rotenberg, Quasiparticle dynamics in graphene, *Nature physics* **3**, 36 (2007).
- [30] J. Martin, N. Akerman, G. Ulbricht, T. Lohmann, J. v. Smet, K. Von Klitzing, and A. Yacoby, Observation of electron-hole puddles in graphene using a scanning single-electron transistor, *Nature physics* **4**, 144 (2008).
- [31] G. Yu, R. Jalil, B. Belle, A. S. Mayorov, P. Blake, F. Schedin, S. V. Morozov, L. A. Ponomarenko, F. Chiappini, S. Wiedmann, *et al.*, Interaction phenomena in

- graphene seen through quantum capacitance, Proceedings of the National Academy of Sciences **110**, 3282 (2013).
- [32] Y. Shao, S. Moon, A. Rudenko, J. Wang, M. Oze-rov, D. Graf, Z. Sun, R. Queiroz, S. H. Lee, Y. Zhu, *et al.*, Semi-Dirac Fermions in a Topological Metal, arXiv preprint arXiv:2311.03735 (2023).